Some considerations on Poincaré maps for chaotic flows

2000 J. Phys. A: Math. Gen. 33 163

(http://iopscience.iop.org/0305-4470/33/1/310)

J. Phys. A: Math. Gen. **33** (2000) 163–170. Printed in the UK PII: S0305-4470(00)07227-9

Some considerations on Poincaré maps for chaotic flows

Wolfram Just† and Holger Kantz

Max-Planck-Institut für Physik Komplexer Systeme, Nöthnitzer Strasse 38, D-01187 Dresden, Germany

E-mail: wolfram@chaos.gwdg.de

Received 26 August 1999

Abstract. The standard way to reduce a flow to a time-discrete dynamical system is by the technique of the Poincaré surface of section. We discuss the relationship between Poincaré maps obtained from different surfaces of section and give some considerations for practical application for this method.

1. Introduction

One century ago Poincaré introduced the concept of time-discrete dynamical systems in his study of two-dimensional autonomous differential equations [1]. Such construction of Poincaré maps has become one of the very basic tools implemented in nonlinear dynamics and is nowadays contained in every textbook on nonlinear dynamics (see, for example, [2]). The method is, to a great extent, used in many applications, for example, at the heart of data analysis [3], control in nonlinear systems [4], and numerical simulations, although one should stress that from the principal point of view the use of Poincaré maps can be frequently avoided. Since the construction of Poincaré maps via a suitable surface of section reduces the dimension of phase space by one, the approach is particularly useful for visualization of three-dimensional complex dynamics. Further dimension reduction can be achieved by a projection along the local stable manifold. For 'nice' (i.e. hyperbolic) dynamical systems such concepts can be formulated, even rigorously, if one considers more complicated topological spaces [5]. Hence, on the one hand Poincaré maps are useful tools in applications and, on the other hand, the concept has a sound mathematical background. For these reasons the understanding of Poincaré maps is at the centre of interest of nonlinear dynamics. To our surprise, we have not been able to find a general and systematic approach in the literature. To our best knowledge, rigorous approaches either consider *local* Poincaré maps which are constructed in the vicinity of a periodic solution of the flow system or *global* maps may be introduced for periodically driven non-autonomous systems such as, for example, kicked rotators. In the latter case the stroboscopic view corresponds to a Poincaré surface of section in the extended phase space at a fixed phase value of the periodic driving term. In numerical investigations, one uses empirical global Poincaré maps for chaotic flows. In the first part of this paper we investigate properties of such global maps, whereas in the second part we give some guidelines for practical purposes and illustrate the properties through experimental data.

† Present address: Max-Planck-Institut für Strömungsforschung, Bunsenstraße 10, D-37073 Göttingen, Germany.

0305-4470/00/010163+08$30.00

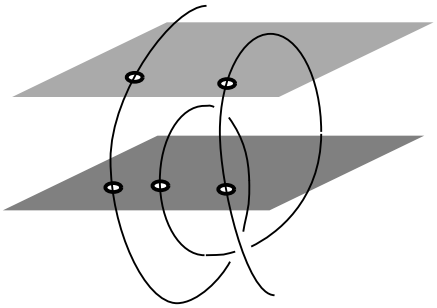

Figure 1. Diagrammatic view of a trajectory in phase space and two different Poincaré cross sections.

Define a time-continuous dynamical system through a first-order differential equation $\dot{z} = f(z)$ in some phase space $\Gamma \subset \mathbb{R}^d$, where f fulfils a Lipschitz condition. The initial value problem thus has a unique solution, which is at least smooth and, through uniqueness, can be followed in both time directions. The Poincaré map is introduced with respect to a given oriented surface of section of co-dimension one in $\mathbb{R}^d$. The action of the map on a point within this surface is defined by considering the trajectory emerging from this point, i.e. of the solution of the initial value problem, and determining the next intersection with the surface *in the predefined orientation*. On the one hand, the initial point belongs to the range of definition of the Poincaré map only, if the trajectory emerging from it has the same orientation. Hence, Poincaré maps are usually not defined on the whole cross section, but only on a subset. On the other hand, the construction of the Poincaré map requires that the trajectory returns with a certain orientation to the surface of section under consideration. Such a property is guaranteed, e.g. in the vicinity of limit cycles where the recurrence follows from standard continuity arguments [5]. In this sense the maps are defined locally. One has to impose additional conditions from the global point of view. Since one is usually interested in the dynamics in the long-time limit, one might restrict the discussion to a suitable ω-limit set, i.e. the set of all points where a trajectory accumulates. In order to ensure that the Poincaré map reflects the complete structure of the flow one has to require that the trajectory on such a limit set crosses the surface of section.

To be more definite consider a topologically mixing and attracting invariant set which contains a dense set of periodic orbits. A suitable globally well-behaving Poincaré map may be defined according to a surface of section such that all periodic orbits intersect transversally with angles bounded from zero. Standard transversality arguments together with the continuity of the flow of the differential equation prove that the Poincaré map does not change up to a smooth conjugacy if such a cross section is deformed slightly (see [6]). One should, of course, keep in mind that without additional topological classification, e.g. along the lines of [7], it is obvious that different Poincaré maps obeying the transversality condition may not be equivalent to each other. In fact, if larger deformations or shifts of the cross section are considered, some part of a trajectory may become tangential to the cross section and, finally, intersection points become lost (see figure 1). Even without expensive analysis several qualitative changes are obvious. The recurrence time of successive intersections of a particular orbit may change discontinuously inducing a corresponding change in local expansion rates and Lyapunov exponents. A period-n orbit of the former map may become a period-$m(\neq n)$ orbit of the latter, and a strange variation of the topological entropy may be caused. Hence, the whole issue deserves a systematic investigation, in particular, if one keeps in mind that in applications it is often impossible to decide whether one has a well-defined global Poincaré map at hand.

2. Transformations in between surfaces of section

To begin with, let us consider a cross section which obeys the above-mentioned transversality condition for all periodic orbits and denote the corresponding Poincaré map by P_0. For simplicity we neglect transients and focus on an invariant set of the dynamics. Such a set determines the range of definition D_0 of the map. By a shift or, more generally, by a smooth deformation of the cross section a whole family of new Poincaré maps P_ε with ranges D_ε is obtained. Here the subscript measures the degree of deformation, i.e. the shift of the cross section. Each point of D_ε is connected to a point of D_0 via the flow of the differential equation if we agree upon whether the flow is considered forward or backward in time, between the different cross sections. From our considerations it is clear that the map P_ε is defined with respect to the domain D_ε. Hence, even if after some deformation the original cross section is recovered the maps P_0 and P_ε need not to be identical since the domains D_0 and D_ε may differ. Such features are related to the global topology of the set under consideration, but we do not intend to dwell on such aspects in what follows. Here we just stress that because of the continuity of the flow a smooth map $h : D_\varepsilon \to D_0$ is induced. Whether h is injective, surjective or both, in some way depends on the just-mentioned topological details of the invariant set. The dynamics of the map P_ε on the set D_ε translates to the dynamics on the image $h(D_\varepsilon) \subseteq D_0$ in such a way that a point $x \in h(D_\varepsilon)$ is iterated with P_0 until it reaches $h(D_\varepsilon)$ again. If we introduce the recurrence map

$$R_\varepsilon(x) := P_0^{N_x}(x) \qquad N_x := \min\{k | P_0^k(x) \in h(D_\varepsilon), k \geqslant 1\} \tag{1}$$

the following commuting diagram is obtained:

$$\begin{array}{ccc} D_0 & \xrightarrow{R_\varepsilon} & D_0 \\ h \uparrow & & h \uparrow \\ D_\varepsilon & \xrightarrow{P_\varepsilon} & D_\varepsilon \end{array} . \tag{2}$$

The diagram tells us that the Poincaré map P_ε is at least as complicated as the recurrence map R_ε on the domain $h(D_\varepsilon) \subseteq D_0$. In particular, one may study aspects of the variation of cross section by means of the original map P_0, without referring to the full phase space of the differential equation. One merely has to consider the recurrence map (1) on a subset of the full domain D_0.

In order to investigate the essential features we first consider a formal model consisting of the Smale complete tent map. For the recurrence map a simple restriction of the phase space is introduced:

$$\begin{aligned} &x' = P_0(x) = 1 - 2|x| \qquad D_0 = [-1, 1] \\ &h(D_\varepsilon) = [-1, 1 - \varepsilon]. \end{aligned} \tag{3}$$

According to our previous discussion the parameter ε mimics the change of the cross section in a fictitious higher-dimensional phase space. The recurrence map (1) is easily computed (see figure 2). As ε increases a symmetric jump develops and wanders for $\varepsilon \in (0, \frac{2}{3})$. This property is quite easy to understand. By shrinking the range of definition from $D_0 = [-1, 1]$ to $h(D_\varepsilon) = [-1, 1 - \varepsilon]$ there appear phase space points x, whose image $P_0(x)$ comes close to the boundary $1 - \varepsilon$. If the image is located to the left, then according to equation (1) x is mapped by P_0, whereas if the image is located to the right, then it is mapped twice: $R_\varepsilon(x) = P_0^2(x)$. Thus the discontinuity appears at the two preimages $P_0^{-1}(1 - \varepsilon)$ of the boundary. In particular, the original period-two orbit $\{-\frac{1}{5}, \frac{3}{5}\}$ of the plain map becomes a period-one orbit of the recurrence map for $\varepsilon \geqslant \frac{2}{5}$. The situation becomes much more intricate if the critical value $\varepsilon = \frac{2}{3}$ is crossed. At the critical value the unstable fixed point of the

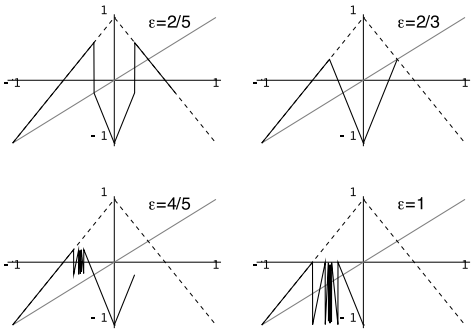

Figure 2. Recurrence map (1) of the tent map (3) for different values of ε (solid line). For comparison the plain map is displayed with broken lines.

plain map leaves the domain of definition $h(D_\varepsilon)$. It is the first time that an unstable orbit is erased completely from the dynamics of the recurrence map. Although the recurrence map becomes continuous at the transition, since both P_0 and R_ε have a common Markov partition, the consequences are quite dramatic. Beyond the transition, $\varepsilon \in (\frac{2}{3}, \frac{6}{5})$, the recurrence map develops a countable infinite number of discontinuities. These discontinuities accumulate at the left preimage of the former fixed point, where the preimage is understood with respect to the plain map P_0. The explanation of such a structure is straightforward. First of all it is evident that something dramatic must happen at the mentioned preimage since this point never returns to $h(D_\varepsilon)$ upon iteration. Strictly speaking, the recurrence map is not defined at this point. Furthermore, points very close to the preimage stay, for a long period of time, close to the former fixed point upon iteration with P_0 until they return to $h(D_\varepsilon)$ because of the topological mixing property. As a consequence, each interval of initial conditions which leaves the domain $h(D_\varepsilon)$ for exactly N iteration steps gives rise to a new branch of the recurrence map. Clearly, these branches accumulate at the above-mentioned preimage. The infinite number of discontinuities cause a blurred structure for the recurrence map. This structure becomes more pronounced if ε decreases. At $\varepsilon = \frac{6}{5}$ the second invariant set of the plain map P_0, i.e. the period-two orbit, leaves the domain $h(D_\varepsilon)$ and the same mechanism repeats. Summarizing, each unstable periodic orbit which is not contained with at least one point in the restricted domain $h(D_\varepsilon)$ gives rise to a countable infinite number of branches in the recurrence map. The same mechanism may be expected to apply for more complicated invariant sets. Through this mechanism the graph of the map acquires a self-similar structure and becomes a fractal curve with a generalized dimension larger than unity. Such a feature is easily understood since the countable infinite number of intervals which support the linear pieces of the graph have widths which decrease exponentially as 2^{-n}. Since the set of numbers $\{2^{-n} | n \in \mathbb{N}\} \subset [0, 1]$ gives rise to a box-counting dimension of one, the total dimension of the graph is two, once the first periodic orbit loses its last intersection point.

Within the present model the recurrence time increases with decreasing ε. Hence, the Lyapunov exponent of the recurrence map increases, since phase space points may be mapped with the original tent map several times. The new exponent may be obtained by simple arguments. As in the case of the plain tent map the invariant density of the recurrence map is uniform as computed straightforwardly from the invariance condition of the corresponding measure $\mu(A) = \mu(R_\varepsilon^{-1}(A))$. A typical orbit of length N of the plain map P_0, contributes a term $N \ln 2$ to the cumulative expansion rate. The same contribution is obtained for the recurrence map, but the length of the sequence is reduced to $N(1 - \varepsilon/2)$ since the orbit visits

the restricted domain $h(D_\varepsilon)$ with frequency $1-\varepsilon/2$ only. Therefore, the Lyapunov exponent of the recurrence map reads $\ln 2/(1-\varepsilon/2)$. According to Pesin's identity [8] the increase of the Lyapunov exponent is accompanied by an increase of the Kolmogorov–Sinai entropy. A similar behaviour might be expected for the topological entropy, in particular, since high-period orbits of the plain map become low-period orbits of the recurrence map. However, no closed analytical expression seems to be available. At the critical value $\varepsilon = \frac{2}{3}$ the topological entropy is simple to calculate since R_ε admits the Markov partition $I_1 = [-1, -\frac{1}{3}]$, $I_2 = [-\frac{1}{3}, 0]$, $I_3 = [0, \frac{1}{3}]$ with possible transitions between all the sets (see figure 2). Hence the transition matrix reads

$$A = \begin{pmatrix} 1 & 1 & 1 \\ 1 & 1 & 1 \\ 1 & 1 & 1 \end{pmatrix} \tag{4}$$

and its largest eigenvalue yields for the topological entropy $h_{\mathrm{top}}(\varepsilon = \frac{2}{3}) = \ln 3$. On the other hand, a divergence of the topological entropy beyond $\varepsilon = \frac{2}{3}$ is expected since the infinite number of branches in the recurrence map may induce an infinite number of fixed points or orbits of low period. To be more definite consider particular periodic orbits of the tent map P_0 which are injected close to the fixed point, stay a certain number of times m in the right-hand interval $x > 0$, and return for one time step to the left branch $x < 0$. It is an easy task to calculate analytically the orbit points, e.g. from its symbolic dynamics $-++\cdots m\text{-times}\cdots+$. For our argument we just need that the trajectory of such an orbit comes very close to the fixed point, in particular in the limit of large m. Put differently, for increasing m only a finite number of orbit points stay outside a neighbourhood of the fixed point. Therefore, each of these orbits generates a periodic orbit of the recurrence map for $\frac{2}{3} < \varepsilon (< \frac{4}{3})$ and the corresponding periods remain finite in the limit $m \to \infty$. In summary, R_ε admits a countable infinite number of periodic orbits of finite period, a divergence of the topological entropy is expected to occur for $\varepsilon > \frac{2}{3}$, and thus the topological entropy develops a jump of infinite height. Last but not least, we mention that even for the highly discontinuous recurrence map the well known inequality between topological and Kolmogorov–Sinai entropy seems to stay valid.

3. Poincaré maps of the Rössler system

The features developed so far on our simple toy model survive in more realistic cases. In particular, it is obvious that any invariant set which is not contained in the cross section causes singularities of the map provided its stable manifold intersects the cross section. In fact, the most prominent, albeit trivial, example for this mechanism is realized by the Lorenz map (see [5]). To illustrate the just-developed nontrivial aspect we resort to numerical simulations of the Rössler system [9]

$$\begin{aligned} \dot{x} &= -y - z \\ \dot{y} &= x + ay \\ \dot{z} &= b + xz - cz \end{aligned} \tag{5}$$

for some standard parameter values $a = 0.15$, $b = 0.2$, $c = 10$. The flow is almost two-dimensional with a numerically unresolvable fractal structure. We restrict the discussion to maps in surfaces of section defined by $x = x_0 = \text{const}$, with intersections from positive to negative values. The first return map of the y variable at the intersections, $y_{n+1} = f_{x_0}(y_n)$, is well defined here for all these surfaces of section. In particular, it is a smooth, one humped map for $x_0 = 0$. The graph of f_{x_0} changes smoothly for decreasing x_0, until at $x_0 \approx -4.3$, parts of the chaotic attractor touch the surface tangentially for the first time. This introduces

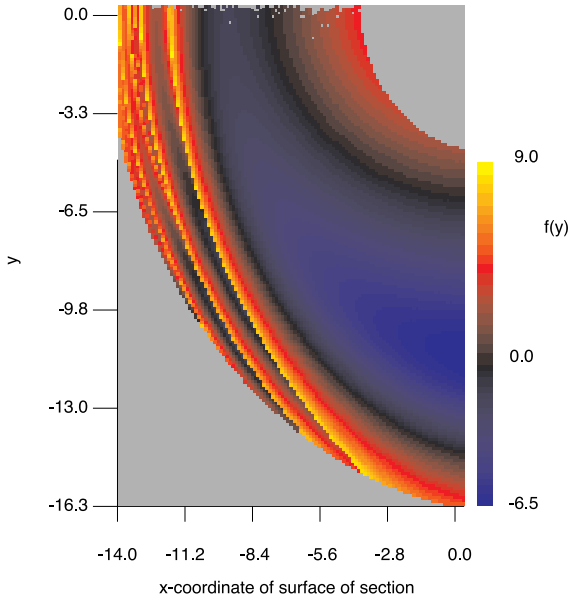

Figure 3. The first return maps $y_{n+1} = f_{x_0}(y_n)$ encoded in greyscale as a function of x_0. The occurrence of the discontinuities is evident as white scars.

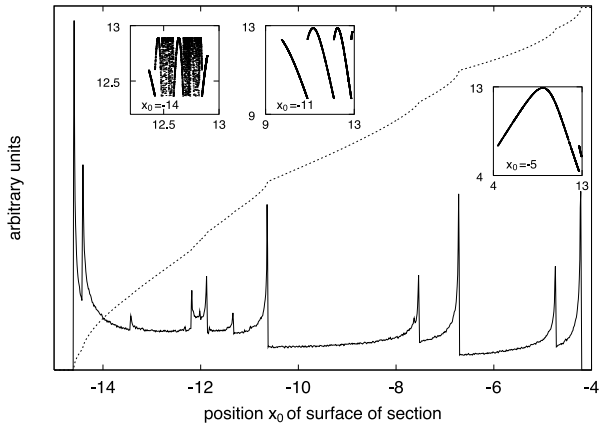

Figure 4. The number of intersections n_{x_0} of a finite Rössler trajectory with the surface of section as a function of its position x_0 (broken curve) and the derivative $\mathrm{d}n_{x_0}/\mathrm{d}x_0$ (solid curve). The insets show graphs of the Poincaré maps at selected values.

the first discontinuity in the map, through the fact that a whole family of long periodic orbits loses one point of intersection. At $x_0 \approx -6.6$ and $x_0 \approx -10.5$ additional discontinuities are introduced (see figure 3). At $x_0 = 14$, as shown by the inset in figure 4, the graph already possesses two families of infinitely many discontinuities, in agreement with the considerations of section 2.

In addition, we have calculated the mean recurrence frequency for the Poincaré maps. For that purpose a fixed finite part of a typical trajectory was considered and the number of intersections n_{x_0} with the cross section $x = x_0$ was computed. Figure 4 shows the result together with its derivative $\mathrm{d}n_{x_0}/\mathrm{d}x_0$. The latter coincides up to some rescaling with the

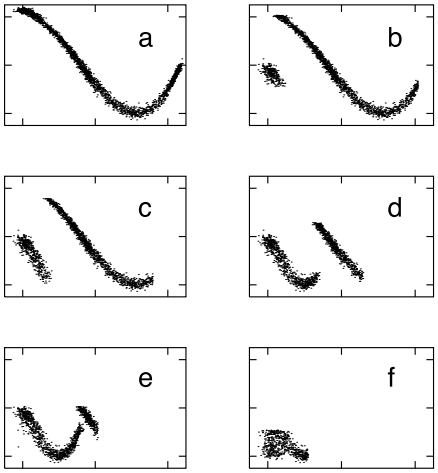

Figure 5. The return maps of the INO-laser data for different cross sections: (*a*)–(*f*) increasing shift ε of the cross section. The maps in (*c*)–(*e*) have two fixed points and in (*f*) potentially infinitely many (see figure 2).

invariant density of the map $f_{x_0=0}$, i.e. n_{x_0} yields the integrated invariant measure. Such a feature is easily understood taking the considerations from section 2 into account. The recurrence frequency is just the probability that a typical orbit stays within the domain $h(D_{x_0})$ upon the iteration with the original map P_0, i.e. $n_{x_0} \sim \mu(h(D_{x_0}))$. In our case the region $h(D_\varepsilon)$ turns out to be an interval where just one of the endpoints depends linearly on x_0.

For sufficiently small x_0, the graph of the Poincaré map itself (see the insets in figure 4) becomes a self-similar fractal object. The function shown for $x_0 = -14$ has a box-counting dimension of $d_{\mathrm{Box}} \approx 1.8$. The arguments of section 2 suggest a value of two, however, logarithmic corrections are expected to occur which reduce the numerically obtained value on finite scales. Despite all these structures, the average return time $\langle T \rangle \sim n_{x_0}$ increases monotonously with decreasing x_0. As it is well known [6], the Lyapunov exponents of the Poincaré maps are related to those of the flow via the the relation $\lambda_{\mathrm{map}} = \lambda_{\mathrm{flow}} \langle T \rangle$, and also the Kolmogorov–Sinai entropy thus increases monotonously, if we assume the validity of Pesin's identity.

4. Experimental data

Finally, let us demonstrate that the same effects are relevant for experimentally obtained Poincaré maps. The underlying data are output intensities of a CO_2 laser system operating at the INO in Firenze [10]. The attractor dimension is again close to two, so that the first return map is essentially one-dimensional (see [11] for details). The fine scale structure which appears when the cross section is shifted and a larger number of discontinuities is introduced is naturally wiped out by measurement noise. Nevertheless, as shown in the sequence of plots in figure 5, when shifting the surface of section, the onset of this scenario can be well observed. For a better comparison of the different Poincaré maps the intersection points were always lifted back to the initial surface of section. Hence, parts of the different graphs are identical, their supports shrink when shifting the surface out of the initial position, and parts of the graph are replaced by higher iterates (see equation (1)).

If visual inspection of the data is possible, a reasonable surface of section should be located such that it intersects the shortest periodic orbit exactly once, and does not miss any orbits of higher period. In practice, this requires one to maximize the number of intersection points derived from the finite experimental data set, under the constraint that they are not artificially increased by a multiple cut of the attractor.

5. Conclusion

We have investigated the influence of the particular cross section on the structure of the resulting Poincaré map. Our analysis revealed that different maps associated with different cross sections are related on some sophisticated level and that strange variations of the Poincaré maps are induced by changing the cross section. In particular, the map may develop discontinuities if some part of the trajectory does not cross the section transversally and a countable infinite number of jumps is generated if some invariant set, such as an unstable periodic orbit, is missed completely.

We have developed these features on a simple analytical model, on numerical simulations of the Rössler model, and on actual experimental data from a laser experiment. As a recipe for the construction of Poincaré maps our analysis indicates that suitable cross section should maximize the number of intersections and that discontinuities in the resulting map should be avoided.

In view of recent suggestions to search for periodic orbits as a signature of determinism in time series data from field measurements [12], our findings suggest investing effort in the optimization of the Poincaré surface of section, since an unsuitable surface can introduce many, in the extreme case infinitely many, fixed points, such that the identification of the fixed points in the presence of noise can become impossible. In particular, Poincaré maps represented by interspike intervals can be unsuitable, if too many small events are ignored [11].

The different Poincaré maps associated with different cross sections are, in general, not conjugated to each other. They are, however, related by the recurrence map as exemplified by our analytical model. As a consequence different quantifiers, such as, for example, Lyapunov exponents, are related to each other if one takes the recurrence time into account.

Our analysis was confined to systems with quasi one-dimensional Poincaré maps for simplicity. We expect that the features developed here persist in higher-dimensional cases although it would be more difficult to detect the analytical structure in these higher-dimensional Poincaré maps explicitly.

Acknowledgments

We thank M Ciofini and R Meucci of the Istituto Nationale di Ottica (INO) in Firenze for supplying us with their excellent experimental data.

References

[1] Poincaré H 1899 *Les Methodes Nouvelles de la Méchanique Céleste* (Paris: Gauthier-Villars)
[2] Schuster H G 1989 *Deterministic Chaos* (Weinheim: VCH)
[3] Kantz H and Schreiber T 1997 *Nonlinear Time Series Analysis* (Cambridge: Cambridge University Press)
[4] Ott E, Grebogi C and Yorke Y A 1990 Control of chaos *Phys. Rev. Lett.* **64** 1196
[5] Guckenheimer J and Holmes P 1986 *Nonlinear Oscillations, Dynamical Systems, and Bifurcations of Vector Fields* (New York: Springer)
[6] Eckmann J P and Ruelle D 1986 Ergodic theory of chaos and strange attractors *Rev. Mod. Phys.* **57** 617
[7] Gilmore R 1998 Topological analysis of chaotic dynamical systems *Rev. Mod. Phys.* **70** 1455
[8] Pesin J B 1976 Lyapunov characteristic exponents and ergodic properties of smooth dynamical systems with an invariant measure *Sov. Math. Dokl.* **17** 196
[9] Rössler O E 1976 An equation for continuous chaos *Phys. Lett.* A **57** 397
[10] Arecchi T F, Gadomski W and Meucci R 1986 Generation of chaotic dynamics by feedback on a laser *Phys. Rev.* A **34** 1617
Ciofini M, Meucci R and Arecchi F T 1995 Experimental control of chaos in a laser *Phys. Rev.* E **52** 94
[11] Hegger R and Kantz H 1997 Embedding of sequences of time intervals *Europhys. Lett.* **38** 267
[12] Pierson D and Moss F 1995 Detecting periodic unstable points in noisy chaotic and limit cycle attractors with applications to biology *Phys. Rev. Lett.* **75** 2124